INORGANIC CHEMISTRY FRONTIERS

RESEARCH ARTICLE

View Article Online
View Journal | View Issue

Cite this: *Inorg. Chem. Front.*, 2023, **10**, 2380

A hollow urchin-like metal–organic framework with Ni–O-cluster SBUs as a promising electrode for an alkaline battery–supercapacitor device†

Tianqi Chen,[a] Sujuan Bian,[a] Xutian Yang,[a] Wenjie Lu,[a] Kuaibing Wang, *[a] Yuxuan Guo,[a] Cheng Zhang[b] and Qichun Zhang *[c,d,e]

A hollow urchin-like Ni-based MOF material (named NiPSC) with long tentacles has been synthesized and directly utilized as an active electrode material in supercapacitors. By virtue of multi-centered Ni-oxo SBU clusters and a large *d*-spacing distance, the pristine NiPSC electrode delivers superior electrochemical performance, including high specific capacity, good rate capability and outstanding cycling stability even under the erosion of an alkaline electrolyte. Moreover, the NiPSC//AC device with NiPSC as the positive electrode and active carbon (AC) as the negative electrode exhibits an excellent capacitance retention of 82.8% after 3000 cycles with a window voltage of 1.7 V, a maximum energy-density value of 28.81 W h kg^{-1} at 425 W kg^{-1}, and potential practicability (two cells can power four LED bulbs for 10 min). Our results suggest that the strategy of modifying the interior structures of MOFs through introducing multiple redox-active sites and adjusting the crystal-lattice distance could effectively improve the performance of the as-obtained materials in supercapacitors.

Received 18th January 2023,
Accepted 10th March 2023

DOI: 10.1039/d3qi00123g

rsc.li/frontiers-inorganic

1. Introduction

Owing to the continuous reduction of fossil fuels and the demand for sustainable energy, the energy-storage grid faces new challenges,[1,2] and advanced eco-friendly energy storage/conversion equipment has been extensively studied.[3] As a class of energy-storage systems, supercapacitors (SCs) with various branches, such as alkaline-ion capacitors, alkaline battery–supercapacitor hybrid devices, micro-supercapacitors and so forth, have been extensively documented.[4–8] Even though great progress in enhancing energy densities has been witnessed in these devices, with current commercially available SCs it remains difficult to meet the energy-consumption requirements of human society. Therefore, developing new strategies to design/prepare novel electrode materials and to fabricate electrodes become crucial for the practical applications of SCs.[9,10]

Currently, metal–organic frameworks (MOFs) have become a class of promising candidate electrode materials for SCs due to their precise chemical compositions at the molecular level, abundant redox-active sites, and enormous "MOF reservoir".[11–15] Through a wide range of research studies, MOF-based electrodes have been demonstrated to be stable in various situations, including acidic, neutral and alkaline environments.[16,17] However, in the process of implementation, the functions of pores and distinct metal nodes/clusters on electrochemical performances have rarely been mentioned or discussed. On the other hand, the defects of normal MOF-based electrodes as active electrodes for long-term recycling, especially the disadvantages of instability and low conductivity, were repeatedly mentioned.[18,19] To address these two points, several strategies, including the combination of conductive materials, the usage of MOFs as templates to fabricate derivative materials, and the improvement of their conductivities, have been widely adopted.[20–22] Furthermore, the formation of bimetallic or trimetallic centers through doping different metals has also been a proven and effective strategy to amend the property defects of MOF-based electrodes, which could further enhance specific capacities, rate capabilities and coulombic efficiencies.[23–26]

These reported results strongly encourage us to investigate the function of redox-active metal–oxide clusters as building units in MOFs because these clusters can be considered as

[a]*Department of Chemistry, College of Sciences, Nanjing Agricultural University, Nanjing 210095, Jiangsu, P. R. China. E-mail: wuhua@njau.edu.cn*
[b]*Nanjing Institute of Environmental Sciences, Ministry of Ecology and Environment, Nanjing 210042, Jiangsu, P. R. China*
[c]*Department of Materials Science and Engineering, City University of Hong Kong, Kowloon, Hong Kong 999077, P. R. China. E-mail: qiczhang@cityu.edu.hk*
[d]*Center of Super-Diamond and Advanced Films (COSDAF), City University of Hong Kong, Hong Kong SAR 999077, China*
[e]*Department of Chemistry, City University of Hong Kong, Kowloon, Hong Kong 999077, P. R. China*

†Electronic supplementary information (ESI) available: Experimental methods, characterization of NiPSC, electeochemical performances of NiPSC, and electrochemical performances of full cells. See DOI: https://doi.org/10.1039/d3qi00123g

multimetal centers. Herein, a MOF-based nanomaterial (named NiPSC) has been prepared through the reaction between the building linker 4,4′,4″-(1,3,5-triazine-2,4,6-triayl) tribenzoic acid (H_3TATB) and $Ni(NO_3)_2$, where unique Ni–O-clusters as SBUs have been formed in the crystalline lattice. Due to these particular Ni–O-cluster sites, the obtained NiPSC has been employed as an active electrode in supercapacitors to evaluate its energy-storage performance. The long cycling stability and structural alteration of NiPSC electrodes in an alkaline environment have also been investigated in sole electrode and alkaline supercapacitor–battery hybrid devices.

2. Results and discussion

The structure of the as-prepared Ni-based MOF (namely NiPSC) was confirmed by powder X-ray diffraction (PXRD), scanning electron microscopy (SEM) and high-resolution transmission electron microscopy (HR-TEM). The PXRD results indicate that all diffraction patterns of the as-obtained powder, even after being fabricated into the active electrode composite, are well matched with the peaks simulated from the single-crystal data $(H_2[Ni_3O(H_2O)_3(TATB)_2]\cdot 5DMF\cdot 2H_2O$, also known as PCN-5),[27] as depicted in Fig. 1a. Its interior structure contains tri-nickel μ_3-oxo-centered SBU clusters that connect six TATB linkers to form a connected network with two kinds of open channels (Fig. 1b and Fig. S1†). This structure also produces multiple active sites. The SEM images confirm that the NiPSC material consists of numerous urchin-like hollow and spherical structures as shown in Fig. 1c and Fig. S2a (for details, see the ESI†). The diameter of the hollow spheres is about 1.5–4 μm (Fig. S2b†). The HR-TEM images further reveal that NiPSC microspheres consist of numerous tentacle structures and the width of the tentacle is about 15–30 nm (Fig. 1d). The crystal lattice of the tentacle structure is clearly observed in the high-resolution TEM image and the typical *d*-spacing width is ~2.14 nm (Fig. 1e), which is close to the diagonal distance of two adjacent Ni–O-cluster centroids (inset of Fig. 1e). The XRD images of a calcined sample of NiPSC, as depicted in Fig. S3,† suggest that the patterns of the calcined sample exactly match the PCPDF pattern (no. 44-1159) of standard patterns of NiO. The obtained NiO material also shows an urchin-like spherical architecture with a short tentacle motif, indicating a good template function of the NiPSC material (Fig. 1f and Fig. S4a, b†). In contrast, the difference between these two materials is that the mean diameter of the spheres and the tentacle length are less than those of the NiPSC template (Fig. 1g and Fig. S5†). According to the HRTEM image in Fig. 1h, the *d*-spacing distance (0.241 nm) of calcined samples could be well assigned to the (111) crystal facet of NiO, in good agreement with the PXRD results.

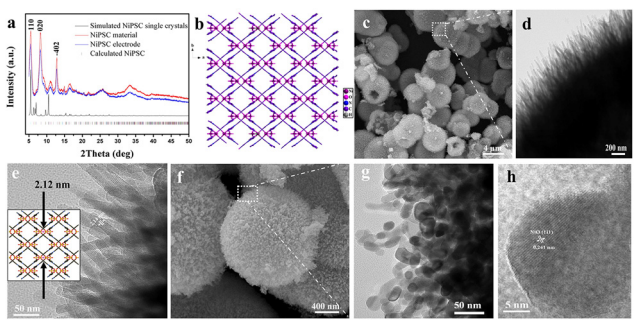

Fig. 1 Structural characterization. (a) PXRD patterns of NiPSC material, electrode and simulated bulk crystals. (b) Crystal structure of NiPSC redrawn from the reported CIF.[27] (c) SEM image of urchin-like NiPSC. (d and e) TEM images of NiPSC at different magnifications. (f) SEM image of NiO. (g and h) TEM images of NiO at distinct magnifications.

X-ray photoelectron spectroscopy (XPS) was then used to identify the surface information and valence state of NiPSC. The survey XPS spectrum confirmed the presence of Ni, C, O, and N elements in the NiPSC material (Fig. S6†). As shown in Fig. S7a,† deconvolution of the C 1s spectrum suggested the existence of C═O (287.8 eV) and C–COOR (288.8 eV) bonds. The strong peaks at 398.8 eV in the N 1s spectrum confirmed that the DMF molecules were embedded into the crystal lattice (Fig. S7b†). Ni 2p analysis shows four components, where two peaks are located at 856.04 and 873.62 eV, attributed to Ni $2p_{1/2}$ and Ni $2p_{3/2}$, respectively, while the other two peaks belong to the satellite peaks of the Ni element (Fig. S7c†).[28] The O 1s peak at 532.1 eV proves the presence of Ni–O cluster bonds or coordinated/lattice water (Fig. S7d†). Besides, energy dispersive spectroscopy (EDS) further confirms the chemical composition of the NiPSC and derived NiO materials, as shown in Fig. S8 and S9.†

The specific surface area, pore volume, and pore size distribution of the as-obtained NiPSC and NiO materials were measured and calculated with the adsorption–desorption curves and pore size distribution diagram, as displayed in Fig. S10.† The adsorption–desorption patterns of NiPSC belong to type IV isotherms. The presence of an H3 mesoporous hysteresis loop indicates the mesoporous structure of the NiPSC material.[29] The specific surface area and pore volume of NiPSC hollow spheres are ~66.70 $m^2\ g^{-1}$ and 0.340 $cm^3\ g^{-1}$, respectively. After the calcination of NiPSC into NiO, the specific surface area, average pore diameter and pore volume all decreased significantly (for details, see Table S1†). Almost no mesopores were observed in the derived NiO material, which could be attributed to the collapse of MOF structures (see the TEM images shown in Fig. S4†).

Through the above-mentioned analyses, the as-obtained NiPSC materials could show potential applications in the energy-storage field due to the unique Ni-oxo-centered SBU clusters with hollow spherical architectures. To confirm whether this idea works, the usage of NiPSC as a working electrode in an alkaline environment was investigated. For comparison purposes, the derived NiO material was also studied as the electrode material.

As shown in Fig. 2a and b, the CV curves indicated that either the NiPSC or NiO electrode displayed evident redox peaks over a potential window of 0–0.6 V, where the oxidation peaks were centered at 0.42–0.52 V and the reduction peaks

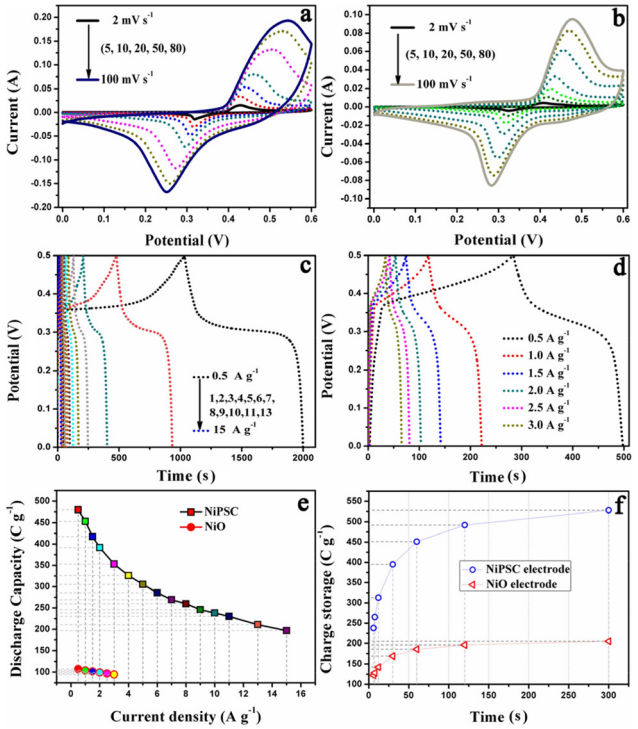

Fig. 2 Electrochemical performances. (a) CV curves of NiPSC. (b) CV curves of the calcined sample. (c) Charge–discharge curves of NiPSC. (d) Charge–discharge curves of the calcined sample. (e) Comparison of the discharge capacitance of the NiPSC electrode and the NiO electrode at the same current density. (f) Comparison of the charge capacitance of the NiPSC electrode and the NiO electrode at the same charging time.

were located at 0.25–0.30 V. Based on the redox motif at various scan rates, the characteristics of battery-type electrode behavior can be inferred for both electrodes,[30,31] resembling the previous reports on Ni-based MOFs or Ni-based oxides/hydroxides.[32,33] For the NiPSC electrode, the redox couple could be attributed to the Ni^{II} and Ni^{III} species,[34] while for the NiO electrode, the chemical process could only happen between the active substance NiO and NiOOH,[35,36] where OH^- in the NiO lattice is replaced by O^{2-} to form a proton defect and the bivalent Ni site is replaced by trivalent Ni to produce an electronic defect. In contrast, the peak currents and integral areas of the NiPSC electrode, calculated from the CV profiles, are much larger than those of the NiO electrode, suggesting that the NiPSC electrode delivers a more superior performance.

The charge–discharge profiles with the obvious plateaus can further confirm the battery-type behaviors of the as-prepared electrodes, as shown in Fig. 2c and d. The charging and discharging processes of NiPSC and NiO showed distinct potential plateau regions, in line with the CV curves. From the discharge time calculation (Fig. 2e), the NiPSC electrode delivered an ultra-high specific capacity of 480 C g^{-1} at a current density of 0.5 A g^{-1}. Even though the current density was increased by 30 times, the capacitance retention of NiPSC still remained at 40.9%, indicating good rate capability. In contrast, the NiO electrode exhibited poor electrochemical performance and the corresponding specific capacity was lower than 110 C g^{-1} (at 0.5 A g^{-1}). This phenomenon could be due to the distinct interior hollow structures with multiple Ni–O-based redox-active centers (Fig. S11†) and the exterior tentacles. As described before, the huge lattice *d*-spacing in the NiPSC tentacles (2.14 nm) facilitates electrons and electrolyte ions reaching the redox centers rapidly, effectively shortening the diffusion path length. Additionally, the hollow structure possesses a sufficient gap/room to accommodate ions, making the resulting specific capacity of NiPSC larger than that of the NiO electrode (filled with nanoparticles).[37,38] The previous BET characterization could also support this deduction. Following careful analyses, NiPSC displayed superior electrochemical performance than NiO electrodes in many aspects. At a constant scanning rate of 2 mV s^{-1} (the charge time is 300 seconds, Fig. 2f), the maximum storage capacity of NiPSC can reach up to 528 C g^{-1}. Under the same charge time, the capacity of the NiO electrode is only ~205 C g^{-1}. When the charge time is as short as 6 seconds, the charge storage achieved by the NiPSC electrode is 238 C g^{-1}, which is still higher than the maximum storage capacity of the NiO electrode (at 300 seconds).

To evaluate the surface contact conditions between the NiPSC electrode and the electrolyte, electrochemical impedance spectroscopy (EIS) measurements were conducted. The plots were simulated as illustrated in Fig. 3a (based on the equivalent circuit as shown in Fig. S12†). The Nyquist data revealed that the series resistance (R_s) of the NiPSC electrode is 0.55 Ω, and the charge-transfer resistance (R_{ct}) is 3.0 Ω, suggesting a lower electrochemical reaction impedance of the

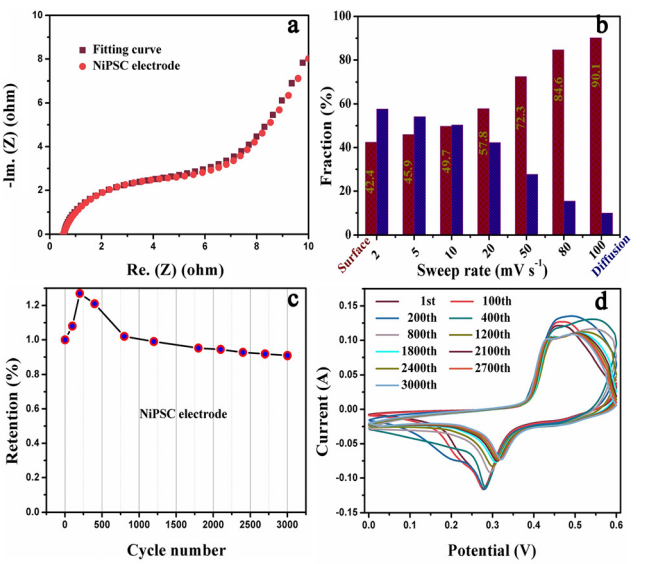

Fig. 3 Mechanism and cycling stability. (a) Nyquist plots of NiPSC. (b) Normalized contribution ratio of surface/diffusion-controlled currents at various scan rates. (c) Capacitance retention of NiPSC in the CV cycling test under the three-electrode system. (d) CV cycling test for NiPSC at 30 mV s^{-1} for 3000 cycles.

Ni-based MOF electrode with multiple Ni–O clusters. In a bid to further analyze the surface contribution to current, surface-controlled and diffusion-dominated sections at various sweep rates were calculated based on Dunn's power-lawer equations (for details, see the ESI†).[39,40] The mimetic *b* values, based on the peak currents, ranged between the values of 0.5 (diffusion-dominated current) and 1.0 (surface-controlled current), illustrating that the electrochemical process of the NiPSC electrode consists of two separate mechanisms simultaneously (Fig. S13†).

These two operating mechanisms can further be simulated quantitatively; at a scan rate of 2 mV s^{-1}, the contributions from the surface capacitive section and diffusion-dominated part are 42.4% and 57.6%, respectively (Fig. S14†). When the sweep rate reaches 100 mV s^{-1}, the achieved surface-controlled contribution to the current is 90.1% (Fig. 3b). At high scan rates, the surface capacitive currents are predominant probably because the diffusion speed of electrolyte ions into the interior active sites is relatively low, which demonstrated once again that NiPSC with its higher specific surface area facilitates the generation of more prominent charge storage capacity.

Under a three-electrode configuration, the cycling performance of the as-fabricated NiPSC electrodes was estimated by adopting CV technology at a constant sweep rate of 30 mV s^{-1} (Fig. 3c). Before 300 cycles, the specific capacity of the electrode displays an obvious upward trend, which could be due to the process of electrode activation, in which the aqueous electrolytes usually take a period to permeate the interior area of the active electrode materials. During this process, the infiltration degree of the NiPSC material into the electrolyte increases. After 300 cycles, the specific capacity of the NiPSC electrode drops sharply. The decline process begins slowly after 800 cycles and the specific capacity retention of the NiPSC electrode remains at 90.9% after 3000 continuous charging–discharging cycles (Fig. 3c). Besides, the structural alteration during this endurance process was also detected by ATR-IR and PXRD (Fig. S13†). The ATR-IR results suggest that the characteristic peaks of samples after 100 cycles and 3000 cycles are consistent with the characteristic peaks of parent NiPSC, respectively (Fig. S15a†). The unchanged chemical compositions of the NiPSC electrode at 100 and 3000 cycles were further proved by PXRD, as shown in Fig. S15b.† The sample has high similarity with the parent NiPSC after 100 cycles and still maintains the main framework intact after 3000 cycles of erosion, showing good electrode stability in alkaline electrolytes. The initial increase in capacity could still be due to the process of electrode activation. This result was in good accordance with the almost unchanged CV curves after 3000 cycles (Fig. 3d).

Based on the excellent performance of the sole electrode, a hybrid supercapacitor–battery energy-storage device with NiPSC as the positive electrode and active carbon (AC) as the negative electrode was investigated (Fig. S16a†). After optimizing the mass relationship between the positive and negative electrode materials, the device, denoted as NiPSC//AC, was assembled and the polarization curves and potential ranges

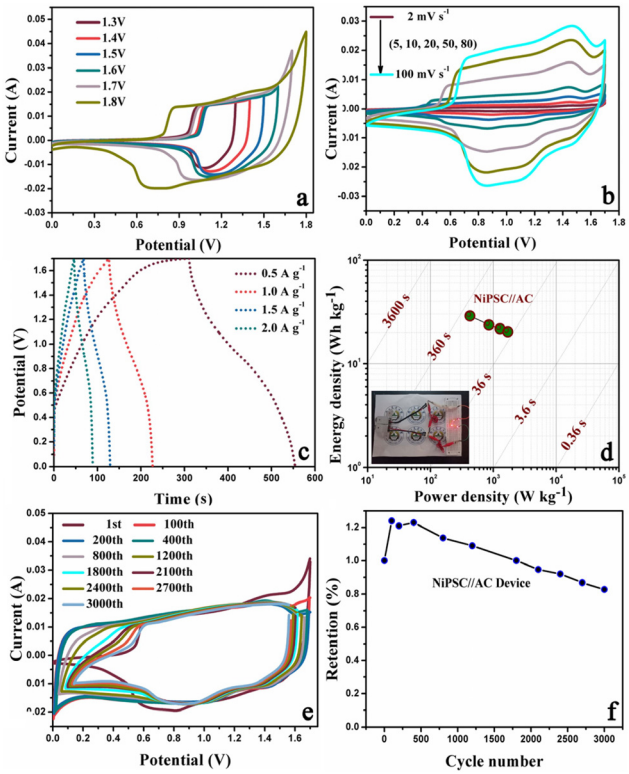

Fig. 4 (a) Polarization curve of NiPSC//AC. (b) CV curve of NiPSC//AC. (c) CP curve of NiPSC//AC. (d) Ragone plots of energy density and power density for NiPSC//AC. Inset: the illumination of red LED bulbs with NiPSC//AC. (e) CV cycling test for NiPSC at 50 mV s^{-1} for 3000 cycles. (f) Capacitance retention of NiPSC in the CV cycling test under the two-electrode system.

were evaluated as depicted in Fig. 4a and Fig. S16b.† By comparing the distorted circumstances of CV curves at various operating potentials, the voltage window for the as-obtained NiPSC//AC device is finally centered at 1.7 V. Under this voltage window, the CV curves of the NiPSC//AC device exhibited typical rectangular shapes at various scan rates, suggesting good reversibility of the device. From the analysis of the discharge branch, the NiPSC//AC device delivered a maximum specific capacitance of 71.8 F g^{-1} at 1.0 A g^{-1}. Under this constant current density, the device can exhibit 28.81 W h kg^{-1} energy density at 425 W kg^{-1} power density, comparable with those in the recent reports (Fig. 4d and Table S2†).[41–46] After assembling the NiPSC//AC device into a button cell, two cells in series can supply power for LED lamps and maintain the illumination of red LED bulbs for up to 10 minutes (inset of Fig. 4d). The electrochemical stability of the NiPSC//AC device was also measured by the cyclic voltammetry method. At a high scan rate of 50 mV s^{-1} within a voltage window of 1.7 V, the CV curves remained unchanged and the capacitance retention of the NiPSC//AC device remained at 82.8% after 3000 charging/discharging cycles (Fig. 4e and f). These superior performances suggest that the NiPSC electrode with Ni–O SBU clusters and hollow motifs could guide the future design of MOF-based electrode materials.

3. Experimental section

The Experimental section can be found in the ESI.†

4. Conclusions

In conclusion, NiPSC nanospheres have been successfully prepared using a tripodal H_3TATB linker and $Ni(NO_3)_2$. The NiPSC electrode has been demonstrated to show excellent specific capacity, and better rate performance and cycling stability in contrast to its derived NiO material. Clearly, without calcination, MOF-based materials with multiple Ni–O redox-active clusters as building units also show potential to be directly used as electrode materials. After being assembled into a hybrid device, NiPSC//AC maintained excellent cycling performance in alkaline environments (82.8% capacitance retention after 3000 cycles). Furthermore, the NiPSC//AC device delivers the highest energy-density value of 28.81 W h kg^{-1} with a power density of 425 W kg^{-1}, which are comparable with those values in recent reports on MOF-based electrodes. These results provide a good strategy for the future design of high-performance MOF-based materials with large pores and multiple redox-active metal-oxo clusters.

Conflicts of interest

There are no conflicts to declare.

Acknowledgements

This work was supported by the National Natural Science Foundation of China (22279061), the Fundamental Research Funds of Central Universities (KYGD202107), and the Natural Science Foundation of Jiangsu Province (BK20180514). Q. Z. expresses gratitude for funding support from the City University of Hong Kong (9380117, 7005620, and 7020040), the Hong Kong Institute for Advanced Study, City University of Hong Kong, Hong Kong, P. R. China, and the State Key Laboratory of Supramolecular Structure and Materials, Jilin University (sklssm202233).

References

1 M. Aneke and M. Wang, Energy storage technologies and real life applications – A state of the art review, *Appl. Energy*, 2016, **179**, 350–377.
2 Y. Li, J. Zhang, Q. Chen, X. Xia and M. Chen, Emerging of Heterostructure Materials in Energy Storage: A Review, *Adv. Mater.*, 2021, **33**, 2100855.
3 E. Pomerantseva, F. Bonaccorso, X. Feng, Y. Cui and Y. Gogotsi, Energy storage: The future enabled by nanomaterials, *Science*, 2019, **366**, 969.
4 S. Dai, Y. Bai, W. Shen, S. Zhang, H. Hu, J. Fu, X. Wang, C. Hu and M. Liu, Core-shell structured Fe_2O_3@Fe_3C@C nanochains and Ni–Co carbonate hydroxide hybridized microspheres for high-performance battery-type supercapacitor, *J. Power Sources*, 2021, **482**, 228915.
5 R. Liu, A. Zhou, X. Zhang, J. Mu, H. Che, Y. Wang, T.-T. Wang, Z. Zhang and Z. Kou, Fundamentals, advances and challenges of transition metal compounds-based supercapacitors, *Chem. Eng. J.*, 2021, **412**, 128611.
6 B. Singh, B. Padha, S. Verma, S. Satapathi, V. Gupta and S. Arya, Recent advances, challenges, and prospects of piezoelectric materials for self-charging supercapacitor, *J. Energy Storage*, 2022, **47**, 103547.
7 K. Wang, S. Wang, J. Liu, Y. Guo, F. Mao, H. Wu and Q. Zhang, Fe-Based Coordination Polymers as Battery-Type Electrodes in Semi-Solid-State Battery-Supercapacitor Hybrid Devices, *ACS Appl. Mater. Interfaces*, 2021, **13**, 15315–15323.
8 Y. Zhang, H.-X. Mei, Y. Cao, X.-X. Yan, J. Yan, H.-X. Gao, H.-W. Luo, S.-W. Wang, X.-D. Jia, L. Kachalova, J. Yang, S.-C. Xue, C.-G. Zhou, L.-X. Wang and Y.-H. Gui, Recent advances and challenges of electrode materials for flexible supercapacitors, *Coord. Chem. Rev.*, 2021, **438**, 213910.
9 S. Kumar, G. Saeed, L. Zhu, K. N. Hui, N. H. Kim and J. H. Lee, 0D to 3D carbon-based networks combined with pseudocapacitive electrode material for high energy density supercapacitor: A review, *Chem. Eng. J.*, 2021, **403**, 126352.
10 Y. Wang, L. Zhang, H. Hou, W. Xu, G. Duan, S. He, K. Liu and S. Jiang, Recent progress in carbon-based materials for supercapacitor electrodes: a review, *J. Mater. Sci.*, 2020, **56**, 173–200.
11 Y. Liu, Z. Ma, H. Niu, Q. Yang, H. Jia and W. Shi, MOF-derived Co_9S_8 polyhedrons on $NiCo_2S_4$ nanowires for high-performance hybrid supercapacitors, *Inorg. Chem. Front.*, 2020, **7**, 4092–4100; K. Wang, Z. Wang, J. Liu, C. Li, F. Mao, H. Wu and Q. Zhang, Enhancing the Performance of Battery-Supercapacitor-Hybrid Energy Device Through Narrowing the Capacitance Difference Between Two Electrodes via the Utilization of 2D MOF-Nanosheet-Derived Ni@nitrogen-Doped-Carbon Core-Shell Rings as Both Negative and Positive Electrodes, *ACS Appl. Mater. Interfaces*, 2020, **12**, 47482–47489; Y. Guo, K. Wang, Y. Hong, H. Wu and Q. Zhang, Recent progress on pristine two-dimensional metal-organic frameworks as active components in supercapacitors, *Dalton Trans.*, 2021, **50**, 11331–11346.
12 R. Freund, O. Zaremba, G. Arnauts, R. Ameloot, G. Skorupskii, M. Dinca, A. Bavykina, J. Gascon, A. Ejsmont, J. Goscianska, M. Kalmutzki, U. Lachelt, E. Ploetz, C. S. Diercks and S. Wuttke, The Current Status of MOF and COF Applications, *Angew. Chem., Int. Ed.*, 2021, **60**, 23975–24001.
13 V. Stavila, A. A. Talin and M. D. Allendorf, MOF-based electronic and opto-electronic devices, *Chem. Soc. Rev.*, 2014, **43**, 5994–6010.
14 D.-G. Wang, Z. Liang, S. Gao, C. Qu and R. Zou, Metal-organic framework-based materials for hybrid super-

capacitor application, *Coord. Chem. Rev.*, 2020, **404**, 213093; Y. Dong, J. Liu, H. Zhang, Q. Li, F. Mao, A. Lu, H. Wu, K. Wang, C. Zhang and Q. Zhang, Novel Isostructural Iron-Series-MOFs Calcined Derivatives as Positive and Negative Electrode: A New Strategy to Obtain Matched Electrodes in Supercapacitor Device, *SmartMat*, 2023, DOI: 10.1002/smm2.1159; K. Wang, Y. Guo and Q. Zhang, Metal-organic frameworks constructed from iron-series elements for supercapacitors, *Small Struct.*, 2022, **3**, 2100115.

15 H. B. Wu and X. W. D. Lou, Metal-organic frameworks and their derived materials for electrochemical energy storage and conversion: Promises and challenges, *Sci. Adv.*, 2017, **3**, eaap9252.

16 S. Kumar, P. H. Weng and Y. P. Fu, Core-shell-structured CuO@Ni-MOF: bifunctional electrode toward battery-type supercapacitors and oxygen evolution reaction, *Mater. Today Chem.*, 2022, **26**, 101159.

17 C. Meng, Y. Cao, Y. Luo, F. Zhang, Q. Kong, A. A. Alshehri, K. A. Alzahrani, T. Li, Q. Liu and X. Sun, A Ni-MOF nanosheet array for efficient oxygen evolution electrocatalysis in alkaline media, *Inorg. Chem. Front.*, 2021, **8**, 3007–3011; C. Li, K. Wang, J. Li and Q. Zhang, Nanostructured potassium-organic framework as an effective anode for potassium-ion battery with a long cycle life, *Nanoscale*, 2020, **12**, 7870–7874.

18 C. Yang, X. Li, L. Yu, X. Liu, J. Yang and M. Wei, A new promising Ni-MOF superstructure for high-performance supercapacitors, *Chem. Commun.*, 2020, **56**, 1803–1806.

19 R. Zhao, Z. Liang, R. Zou and Q. Xu, Metal-Organic Frameworks for Batteries, *Joule*, 2018, **2**, 2235–2259.

20 B. Hosseinzadeh, B. Nagar, R. Benages-Vilau, P. Gomez-Romero and S. H. Kazemi, MOF-derived conformal cobalt oxide/C composite material as high-performance electrode in hybrid supercapacitors, *Electrochim. Acta*, 2021, **389**, 138657.

21 S. Wang, S. Wang, X. Guo, Z. Wang, F. Mao, L. Su, H. Wu, K. Wang and Q. Zhang, An asymmetric supercapacitor with an interpenetrating crystalline Fe-MOF as the positive electrode and its congenetic derivative as the negative electrode, *Inorg. Chem. Front.*, 2021, **8**, 4878–4886.

22 J. Zhang, Y. Li, M. Han, Q. Xia, Q. Chen and M. Chen, Constructing ultra-thin Ni-MOF@NiS_2 nanosheets arrays derived from metal organic frameworks for advanced all-solid-state asymmetric supercapacitor, *Mater. Res. Bull.*, 2021, **137**, 111186.

23 Y. Chen, D. Ni, X. Yang, C. Liu, J. Yin and K. Cai, Microwave-assisted synthesis of honeycomblike hierarchical spherical Zn-doped Ni-MOF as a high-performance battery-type supercapacitor electrode material, *Electrochim. Acta*, 2018, **278**, 114–123.

24 K. Wang, H. Wang, R. Bi, Y. Chu, Z. Wang, H. Wu and H. Pang, Controllable synthesis and electrochemical capacitor performance of MOF-derived MnO_x/N-doped carbon/MnO_2 composites, *Inorg. Chem. Front.*, 2019, **6**, 2873–2884.

25 C. Feng, C.-P. Lv, Z.-Q. Li, H. Zhao and H.-H. Huang, A porous 2D Ni-MOF material with a high supercapacitive performance, *J. Solid State Chem.*, 2018, **265**, 244–247.

26 M. Yang, L. Jiao, H. Dong, L. Zhou, C. Teng, D. Yan, T.-N. Ye, X. Chen, Y. Liu and H.-L. Jiang, Conversion of bimetallic MOF to Ru-doped Cu electrocatalysts for efficient hydrogen evolution in alkaline media, *Sci. Bull.*, 2021, **66**, 257–264.

27 S. Ma, X. S. Wang, E. S. Manis, C. D. Collier and H. C. Zhou, Metal-organic framework based on a trinickel secondary building unit exhibiting gas-sorption hysteresis, *Inorg. Chem.*, 2007, **46**, 3432–3434.

28 X. Zhang, W. Lu, Y. Tian, S. Yang, Q. Zhang, D. Lei and Y. Zhao, Nanosheet-assembled NiCo-LDH hollow spheres as high-performance electrodes for supercapacitors, *J. Colloid Interface Sci.*, 2022, **606**, 1120–1127.

29 S. Gao, Y. Sui, F. Wei, J. Qi, Q. Meng and Y. He, Facile synthesis of cuboid Ni-MOF for high-performance supercapacitors, *J. Mater. Sci.*, 2018, **53**, 6807–6818.

30 V. Augustyn, J. Come, M. A. Lowe, J. W. Kim, P. L. Taberna, S. H. Tolbert, H. D. Abruna, P. Simon and B. Dunn, High-rate electrochemical energy storage through Li^+ intercalation pseudocapacitance, *Nat. Mater.*, 2013, **12**, 518–522.

31 K. Wang, Q. Li, Z. Ren, C. Li, Y. Chu, Z. Wang, M. Zhang, H. Wu and Q. Zhang, 2D Metal-Organic Frameworks (MOFs) for High-Performance BatCap Hybrid Devices, *Small*, 2020, **16**, 2001987.

32 G. Guo, Direct fabrication of mixed metal–organic frameworks (Ni/Cu-MOF) and C@$NiCu_2O_4$ onto Ni foam as binder-free high performance electrode for supercapacitors, *J. Mater. Sci.: Mater. Electron.*, 2021, **32**, 16287–16301.

33 J. Wang, Q. Zhong, Y. Xiong, D. Cheng, Y. Zeng and Y. Bu, Fabrication of 3D Co-doped Ni-based MOF hierarchical micro-flowers as a high-performance electrode material for supercapacitors, *Appl. Surf. Sci.*, 2019, **483**, 1158–1165.

34 Y. Li, Y. Xu, Y. Liu and H. Pang, Exposing 001 Crystal Plane on Hexagonal Ni-MOF with Surface-Grown Cross-Linked Mesh-Structures for Electrochemical Energy Storage, *Small*, 2019, **15**, 1902463.

35 L. Wang, Y. Jiao, S. Yao, P. Li, R. Wang and G. Chen, MOF-derived NiO/Ni architecture encapsulated into N-doped carbon nanotubes for advanced asymmetric supercapacitors, *Inorg. Chem. Front.*, 2019, **6**, 1553–1560.

36 H. Xiao, F. Qu and X. Wu, Ultrathin NiO nanoflakes electrode materials for supercapacitors, *Appl. Surf. Sci.*, 2016, **360**, 8–13.

37 S. Devaraj and N. Munichandraiah, Effect of Crystallographic Structure of MnO_2 on Its Electrochemical Capacitance Properties, *J. Phys. Chem. C*, 2008, **112**, 4406–4417.

38 K. Wang, R. Bi, M. Huang, B. Lv, H. Wang, C. Li, H. Wu and Q. Zhang, Porous Cobalt Metal-Organic Frameworks as Active Elements in Battery-Supercapacitor Hybrid Devices, *Inorg. Chem.*, 2020, **59**, 6808–6814.

39 Y. Jiao, J. Pei, C. Yan, D. Chen, Y. Hu and G. Chen, Layered nickel metal–organic framework for high performance alkaline battery-supercapacitor hybrid devices, *J. Mater. Chem. A*, 2016, **4**, 13344–13351.
40 J. Wang, J. Polleux, J. Lim and B. Dunn, Pseudocapacitive Contributions to Electrochemical Energy Storage in TiO_2 (Anatase) Nanoparticles, *J. Phys. Chem. C*, 2007, **111**, 14925–14931.
41 Y. Li, L. Cao, L. Qiao, M. Zhou, Y. Yang, P. Xiao and Y. Zhang, Ni–Co sulfide nanowires on nickel foam with ultrahigh capacitance for asymmetric supercapacitors, *J. Mater. Chem. A*, 2014, **2**, 6540–6548.
42 Y. Liu, Y. Wang, Y. Chen, C. Wang and L. Guo, NiCo-MOF nanosheets wrapping polypyrrole nanotubes for high-performance supercapacitors, *Appl. Surf. Sci.*, 2020, **507**, 145089.
43 D. Xiong, M. Gu, C. Chen, C. Lu, F. Yi and X. Ma, Rational design of bimetallic metal–organic framework composites and their derived sulfides with superior electrochemical performance to remarkably boost oxygen evolution and supercapacitors, *Chem. Eng. J.*, 2021, 404–127111.
44 S. Zhao, H. Wu, Y. Li, Q. Li, J. Zhou, X. Yu, H. Chen, K. Tao and L. Han, Core–shell assembly of carbon nanofibers and a 2D conductive metal–organic framework as a flexible free-standing membrane for high-performance supercapacitors, *Inorg. Chem. Front.*, 2019, **6**, 1824–1830.
45 N. L. W. Septiani, Y. V. Kaneti, K. B. Fathoni, J. Wang, Y. Ide, B. Yuliarto, Nugraha, H. K. Dipojono, A. K. Nanjundan, D. Golberg, Y. Bando and Y. Yamauchi, Self-assembly of nickel phosphate-based nanotubes into two-dimensional crumpled sheet-like architectures for high-performance asymmetric supercapacitors, *Nano Energy*, 2020, **67**, 104270.
46 S. Gao, Y. Sui, F. Wei, J. Qi, Q. Meng, Y. Ren and Y. He, Dandelion-like nickel/cobalt metal-organic framework based electrode materials for high performance supercapacitors, *J. Colloid Interface Sci.*, 2018, **531**, 83–90.